JETIR.ORG ISSN: 2349-5162 | ESTD Year : 2014 | Monthly Issue
JOURNAL OF EMERGING TECHNOLOGIES AND INNOVATIVE RESEARCH (JETIR)
An International Scholarly Open Access, Peer-reviewed, Refereed Journal

ANALYSIS OF SOLAR AIR HEATER WITH HALF-PERFORATED BAFFLES

YAJJALA SIRISHA, P. S. KISHORE

Department of Mechanical Engineering

Andhra University College of Engineering, Visakhapatnam 530003, India.

Abstract

Enhancing the efficiency of traditional solar air heaters with reduced thermal performance can be accomplished by integrating small perforated baffles on the airflow side of the heat-absorbing plate. This article presents the results of a comparative investigation that utilizes both analytical and numerical approaches. The research involves showcasing a performance chart for the air heater with ducts containing baffles, which is produced through a mathematical model. Additionally, the influence of various environmental factors on the expected thermal efficiency is studied. The utilization of ANSYS Fluent facilitates Computational Fluid Dynamics (CFD) simulations. Several mass flow rates ranging from 0.02 to 0.10 are employed to evaluate heat gain and thermal efficiency. The flow pattern within the system is characterized as laminar. The obtained outcomes reveal a significant agreement between the conclusions drawn from the analytical and numerical methodologies.

Keywords: Solar air heater, duct with baffles, heat gain and CFD.

1. Introduction

In recent times, the practice of enhancing convective heat transfer within rectangular ducts has become quite commonplace through the use of baffles or ribs. This method has found widespread application in improving the thermo-hydrodynamic efficiency of various industrial processes. These processes include thermal power generation, heat exchange operations, air conditioning systems, refrigeration units, chemical processing facilities, automotive radiators, and solar air heaters.

Solar air heaters are devices crafted to raise air temperature by harnessing solar energy as a heat source. These devices are known for their affordability, simple design, minimal maintenance needs, and eco-friendly characteristics. As a result, they are extensively employed for tasks such as timber drying, agricultural product dehydration, space heating, solidifying clay/concrete building components, and curing industrial products.

The conventional setup of a solar air heater comprises a rectangular duct housing an absorber plate placed at the top, a rear plate, insulation beneath the rear plate, a solar-exposed glass cover, and an air passage between the lower plate and the absorber to facilitate airflow. A detailed illustration of the construction elements of a solar air heater can be found in Figure 1.1.

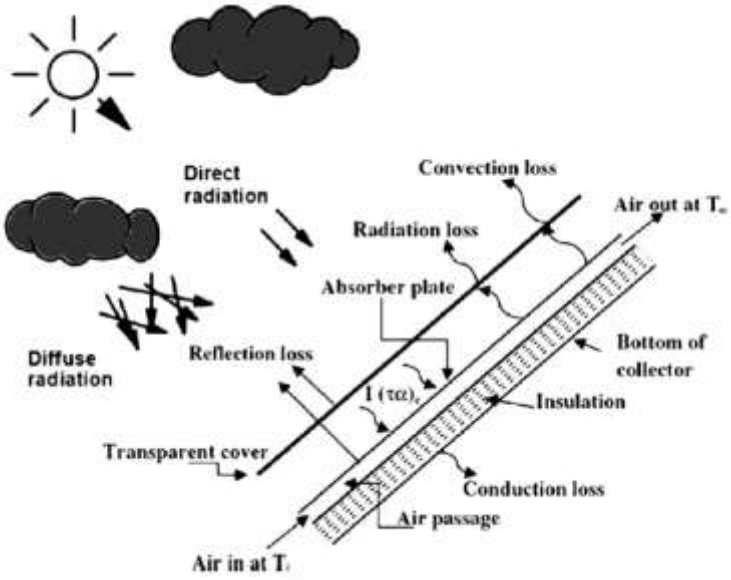

Fig: Solar air heater constructional details.

Prasad et al. [1] suggested that achieving a temperature rise of 3-6°C was sufficient for drying cereal grains. They carried out experiments using an unglazed rectangular duct, which included an absorber plate at the top and protruding wires just below it. The purpose of these wires was to investigate their influence on friction properties and heat transfer characteristics within their solar air heater. The heat transfer coefficients they measured aligned well with established theoretical relationships. Importantly, they observed that incorporating protruding wires beneath the absorber plate increased the efficiency of the unglazed collector from 0.63 to 0.72 at a Reynolds number of 40,000.

In a separate study, Prasad et al. [2] assessed the performance of fully developed turbulent flow within an asymmetrically heated solar air heater duct. They introduced protruded wires beneath the collector plate and developed correlations for calculating average friction factor and average Stanton number. Their calculated friction factor values deviated by an average of 6.3%, and their Nusselt number results deviated by 10.7% from available data. They concluded that adding roughness to the absorber plate contributed to improved heat transfer as well as increased friction factor. They evaluated performance using two parameters: relative roughness height and relative roughness pitch. Increasing the relative roughness pitch led to a decrease in heat transfer rate and an increase in friction factor, while both friction factor and heat transfer decreased with higher relative roughness pitch.

Prasad and Saini et al. [3] aimed to optimize flow and roughness parameters to enhance heat transfer while minimizing friction factor. They explored a range of parameters and identified a specific roughness Reynolds number that offered optimal thermo-hydraulic conditions. The Nusselt number increased with higher Reynolds numbers, while the opposite trend was observed for the friction factor. Optimal conditions were achieved when roughness height slightly exceeded the thickness of the transition sublayer. They developed design curves to assist in selecting parameters for achieving optimal thermo-hydraulic performance.

Sarma et al. [4] theoretically predicted wall friction coefficients and Nusselt numbers, which showed reasonable agreement with established solutions such as the Blasius wall friction coefficient and Dittus and Boelter heat transfer correlation. The predicted Nusselt numbers using eddy diffusivity expressions also matched well with the Dittus and Boelter correlation. Additionally, the analysis could be adjusted by modifying the correction factor to align with predictions from the Petukhov–Gnielinski correlation.

Kishore [5] made predictions for friction factors and convective heat transfer coefficients using twisted tapes within a tube. These predictions covered a wide range of Reynolds numbers and Prandtl numbers. The presence of the tape in the flow was found to possibly lead to a gradual transition from laminar to turbulent flow. A combined friction coefficient correlation applicable across a wide range of Reynolds numbers was extended to theoretically predict convective heat transfer coefficients, with the notion that a clear laminar-to-turbulent flow transition might not be evident.

Sarma et al. [6] conducted an experiment to predict momentum and thermal diffusivities using Al2O3 nanofluid in order to develop Nusselt number and friction factor correlations. The enhancement of convective heat transfer was attributed to the presence of nanoparticles in water. They introduced an improved method for evaluating both eddy momentum and thermal diffusivities as functions of dimensionless velocity and distance.

The solar ducts are constructed in compliance with the ASHRAE Standard for assessing solar collectors. Each duct has a length of 2000 mm, comprising insulated entry and exit segments, each measuring 1000 mm, with a central test portion of 1.62 m. The fixed height for both ducts is 38.4 mm, and the combined width, including the side walls, is 850 mm. In the test section of one duct, there exists an aluminum plate with a thickness of 3.25 mm, divided into 12 equally wide sections, serving as the absorber plate. Additionally, twelve aluminum baffles, each 0.9 mm thick, are placed in between these sections. Each baffle contains a row of holes, as shown in Figure 1(a). The second duct holds an aluminum absorber plate with a smooth surface, divided into three sections. The solar-exposed surfaces of both absorber plates are coated in black for optimal absorption. A 4 mm thick glass plate acts as a cover over the absorber plates, positioned 60 mm above them. The upper side of the entry and exit sections in each duct is covered by plywood.

To ensure a uniform exit air temperature in the measurement section immediately after the mixing part, a baffled mixing section of 100 mm is integrated. At the exit of each duct, a rectangular-to-circular transition piece connects to a galvanized iron (G.I.) pipe with an inner diameter of 68 mm, housing an orifice plate assembly. The orifice plate has a throat diameter of 38 mm. The other end of each pipe connects to the suction of a 10 HP blower through flexible piping and a Y-section, with a control valve for regulation. Insulation with a thickness of 50 mm, in the form of a thermocouple, is applied at the back of the collector, covering the area from the inlet of the test section to the outlet of the twin duct. Insulation in the shape of a foam blanket covers the transition pieces and the pipes of the orifice plate assembly up to the orifice plates. Adequate sealing using putty is applied to all joints. The setup is horizontally positioned (facing north-south) on the rooftop at a height of 750 mm, supported by an iron stand.

Width of the Duct, W = 1m

Length of the Duct, L = 2m

Height of the Duct, H = 35mm = 0.035m

2. CFD modelling

The configurations utilized in this investigation are chosen in accordance with the information gathered from the literature survey. The ANSYS Design Modeler is utilized to establish the geometric model, facilitating rapid modifications when needed. Initially, the ANSYS Workbench interface is initiated, unveiling a variety of solvers and analysis alternatives situated on the left side. The selection is made for flow analysis using FLUENT, encompassing tasks such as geometry manipulation, meshing, solving, analysis, and interpretation of results.

The geometry is brought into this interface from an IGES file that is generated using CATIA software.

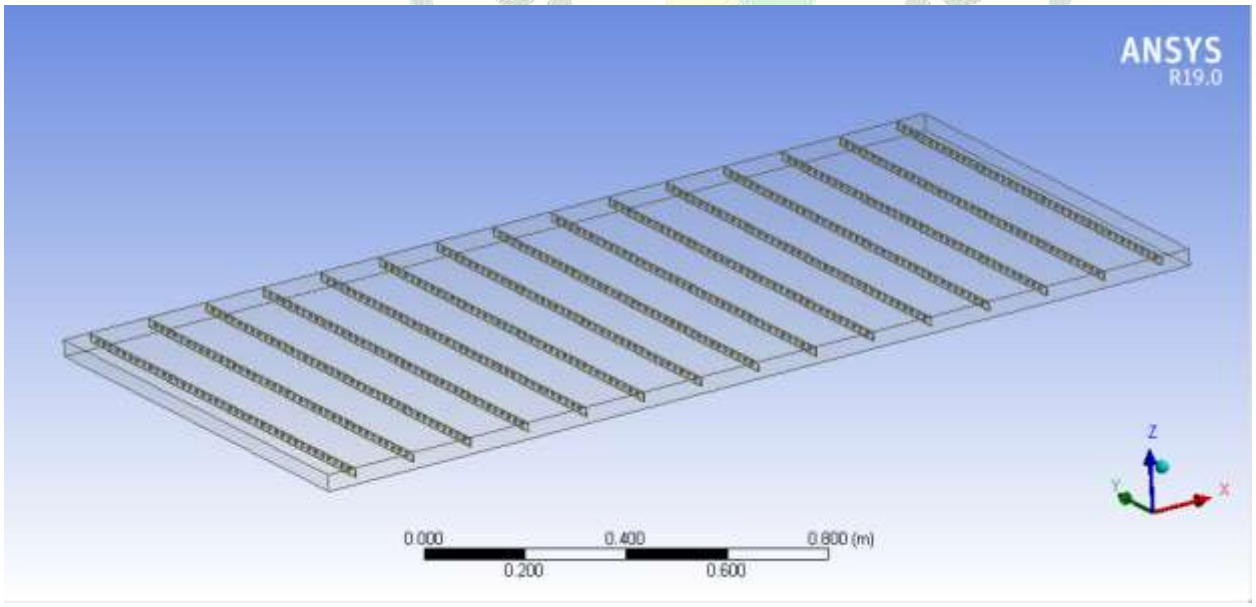

Fig 4.4: Geometry model of duct with baffles.

After the model is prepared, the next phase entails generating the mesh. The material for the complete domain is specified as "FLUENT," and each boundary within the domain is identified for partitioning, with the goal of forming a hexagonal mesh arrangement. By performing a right-click on the "mesh" choice, the creation menu becomes accessible, and the meshing process is initiated through this selection.

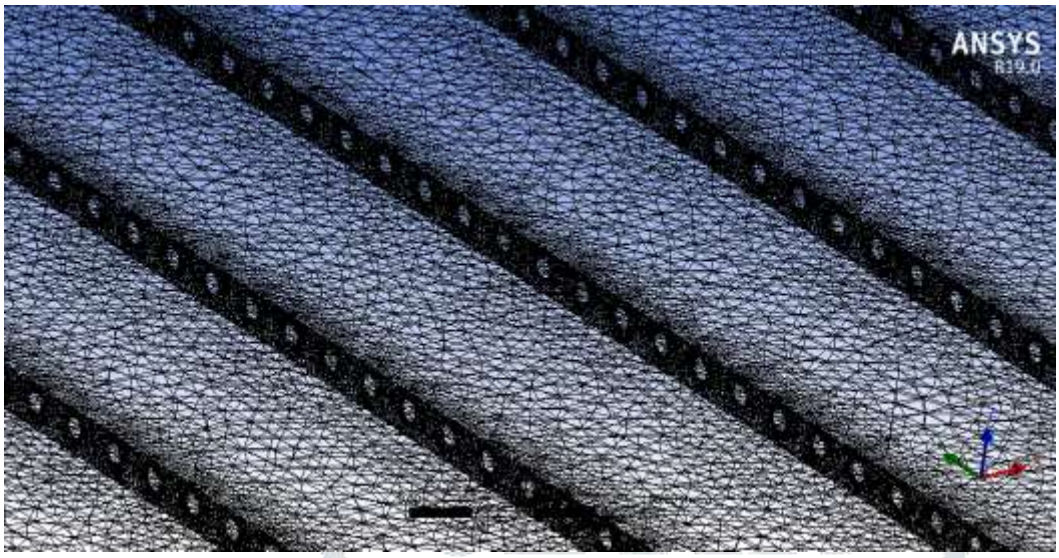

Fig: Meshed model detail view.

In the Air region, various surfaces are assigned labels like inlet, outflow, side, adiabatic, and heat. These labels serve a valuable purpose within the FLUENT software, assisting in the definition of boundary conditions. This emphasis is highlighted in the provided illustration through the use of red markings. To assign a label to a surface, you simply need to right-click on it, access the "name" section, and input the appropriate designation.

For every analysis run, a standard initialization starting from the inlet is utilized. This process streamlines the initialization of all directly related variables using initial approximations. This encompasses parameters such as x and y velocities, temperature, and pressure. Other variables are maintained as constants across the entire domain.

Once the previous steps are completed, it is time to execute the analysis. The FLUENT software will progressively solve the problem until a converged solution is reached. The convergence of the solution is dependent on factors like geometry, node and element count. For this particular study, the selected criteria for convergence involve achieving a velocity convergence of 10^-5 in the x, y, and z directions, along with addressing turbulence and continuity. However, in this specific study, different models – with and without coating – achieved convergence around the 350th iteration.

3. Mathematical modelling

Hydraulic Depth :

$$D_H = \frac{4WH}{2(W+H)} \quad \text{.....(1)}$$

Dynamic Viscosity,$\mu = 1.81 \times 10^{-5}$

Gap between Absorber Plate and Glass Cover, $\delta = 0.05m$

Transmittance-Absorptance product, $T_\alpha = 0.8$

Thickness of Glass Cover, $t_g = 0.004m$

Thermal Conductivity of Glass Cover, $k_g = 0.78 Wm^{-1}K^{-1}$

Back Insulation Thickness, $t_c = 0.05m$

Thermal Conductivity of Back Insulation Material, $k_i = 0.037 Wm^{-1}K^{-1}$

Area:

$A = LxW$

Thermal Conductivity of Air, k = 0.0262 $Wm^{-1}K^{-1}$

Area of the edge of the air heater:

$$A_e = \frac{3(H+t_g+t_c)}{3W} \quad \text{.....(2)}$$

Edge Loss:

$$Q_e = 0.5A_e(T_p - T_a) \quad \text{.....(3)}$$

Wind Heat Transfer Coefficient, $h_w = 5 Wm^{-2}K^{-1}$

Back Insulation Thickness for Glass Cover, $\varepsilon_g = 0.88$

Stefan Boltzmann Constant, $\sigma = 5.67 \times 10^{-8} W/m^2K^4$

Heat Transfer from absorber plate:

$$Q_{tpg} = A\left[\sigma\varepsilon_g\left({T_g}^4 - {T_s}^4\right) + h_w(T_g - T_a)\right] \quad \text{------(4)}$$

$$T_b = \frac{T_p + T_a}{2}$$

Longwave Emissivity Values

$\varepsilon_g = 0.9$

$\varepsilon_b = 0.9$

Heat Transfer by Radiation from the heated absorber plate to the duct bottom surface:

$$Q_{pb} = \sigma\left({T_p}^4 - {T_b}^4\right)\left(\frac{1}{\varepsilon_p} + \frac{1}{\varepsilon_b} - 1\right)^{-1} \quad \text{--------(5)}$$

$$Q_{ba} = \frac{(T_b - T_a)}{\left(\frac{\delta}{k_i} + \frac{1}{h_w}\right)} + h(T_b - T_m) \quad \text{--------(6)}$$

Back and Edge Loss or Back Loss:

$$Q_b = \frac{A(T_b - T_a)}{\left(\frac{\delta}{k_i} + \frac{1}{h_w}\right)} \quad \text{--------(7)}$$

Solar Insolation, I = 800Wm^{-2}

$$Q_L = Q_e + Q_{tpg} + Q_b$$

$$Q = AIT_\alpha - Q_L$$

$$U_L = \frac{Q_L}{A(T_p - T_a)}$$

$$Re = \frac{GD_H}{\mu}$$

$$G = \frac{m}{A}$$

$$m = G\ x\ A$$

$$Nu = 5.385 + 0.148Re\left(\frac{H}{L}\right)$$

$$T_o = T_i + \frac{Q}{mc_p}$$

$$f = \frac{24}{Re} + \frac{\left(0.64 + (38/Re)\right)D_H}{4L}$$

Pressure Loss:

$$\delta_p = \left(\frac{4fL}{2\rho D_H}\right)\left(\frac{m}{WH}\right)^2$$

$$Q = hA(T_o - T_i)$$

$$h = \frac{Q}{A(T_o - T_i)}$$

$$Q = mc_p(T_o - T_i)$$

$$\eta = \frac{Q}{A_a xI}$$

Results and Discussion

The average heat transfer coefficient area can be witnessed for both the flat tube and fluid heat transfer coefficient, yielding a measurement of 19.79 W/m².

Fig: 4.16 Temperature distribution on plane tube

The mean temperature difference area is discernible from this image. More precisely, the entry temperature measures 285 K, while the exit temperature is 357.15 K.

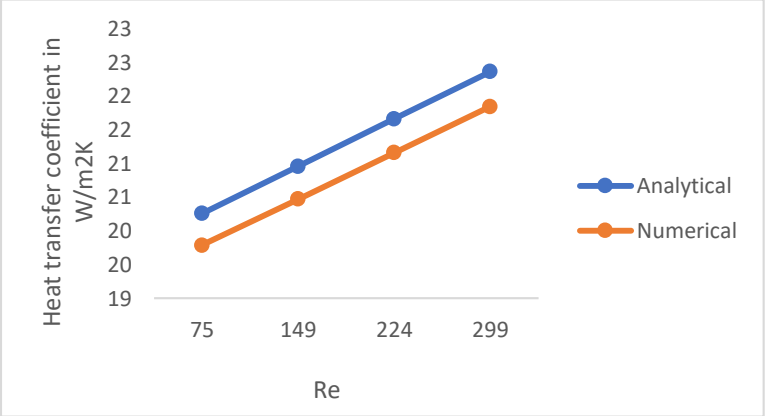

Fig: Heat transfer coefficient with Re.

The heat transfer coefficient holds significant importance in the realm of heat transfer, serving as a fundamental parameter that describes a material's or fluid's capacity to conduct heat. It quantifies the pace at which heat moves between two surfaces featuring a temperature disparity. The graph above illustrates the relationship between the heat transfer coefficient and the Reynolds number. The graph displays both analytical and numerical outcomes. It's evident that as the Reynolds number escalates, the heat transfer coefficient also increases, a trend observed in both sets of results. Within the analytical results, the peak heat transfer coefficient emerges at a Reynolds number of 299, registering at 21 for the analytical data and 22 for the numerical data.

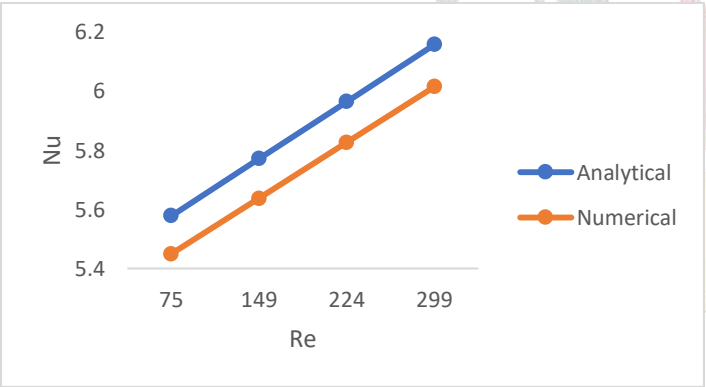

Graph: Nu with Re.

The Nusselt number (Nu) is a dimensionless number used in the field of heat transfer to characterize the convective heat transfer of a fluid flowing over a surface. It relates the heat transfer rate due to convection to the heat transfer rate that would occur purely due to conduction. The graph provided illustrates the variation of the Nusselt number in relation to the Reynolds number. Both analytical and numerical outcomes are depicted within the graph. It is evident that as the Reynolds number escalates, the Nusselt number similarly experiences an augmentation. This trend is consistent across both the analytical and numerical findings. In terms of the analytical results, the peak Nusselt number is observed at a Reynolds number of 299, registering at 6.1. In contrast, the numerical analysis yields a slightly lower value of 5.9 for the same Reynolds number.

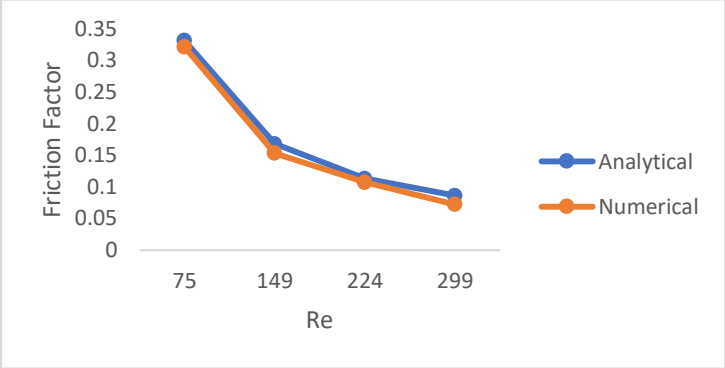

Graph: Friction factor with Re.

The friction factor, often denoted as "f," is a dimensionless parameter used in fluid dynamics to quantify the resistance to flow in a pipe or conduit. It is a fundamental parameter in the analysis of pressure drop or head loss in fluid systems, especially in cases of fluid flowing through pipes, channels, or ducts. The graph provided illustrates the variation of the friction factor in relation to the Reynolds number. Both analytical and numerical outcomes are depicted within the graph. It is evident that as the Reynolds number escalates, the friction factor reduced and is consistent across both the analytical and numerical findings and vice versa. In terms of the analytical results, the peak the friction factor is observed at a Reynolds number of 299, registering at 0.12. In contrast, the numerical analysis yields a slightly lower value of 0.1 for the same Reynolds number.

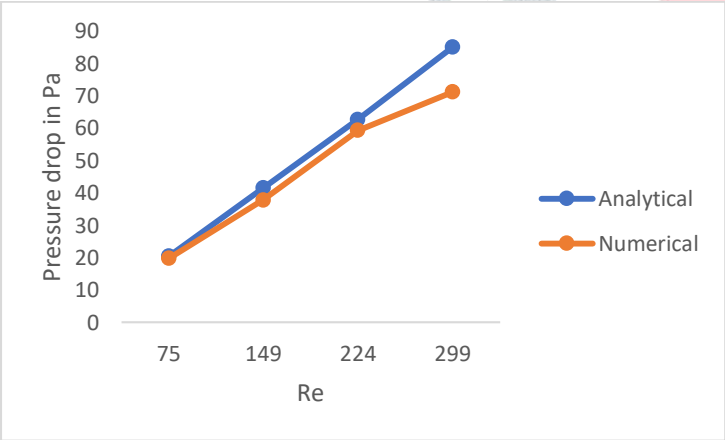

Fig: Pressure drop with Re.

Pressure drop, commonly known as head loss, pertains to the decrease in fluid pressure encountered during its passage through a conduit, encompassing pipes, ducts, or channels. This reduction in pressure arises from a multitude of factors, including the effects of friction, alterations in elevation, and shifts in fluid velocity. The graphic representation portrays the relationship between Pressure drop and the Reynolds number. The chart showcases both analytical and numerical outcomes. As discerned from the graph, an escalation in the Reynolds number corresponds to an amplification in Pressure drop. This trend holds consistent for both the analytical and numerical data. Notably, the analytical results highlight a pinnacle Pressure drop transpiring at a Reynolds number of 299, quantified at 80 units. In comparison, the numerical analysis yields a slightly lower figure of 70 for the equivalent Reynolds number.

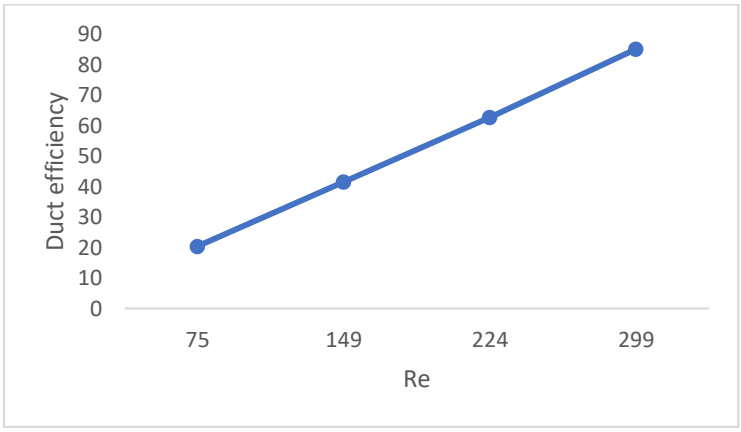

Fig: Duct efficiency with Re.

Duct efficiency refers to the effectiveness of a duct system in conveying air or fluid from one location to another while minimising energy losses, pressure drops, and other inefficiencies. In HVAC (heating, ventilation, and air conditioning) systems and industrial applications, ducts are crucial in distributing air or gases to desired areas. Duct efficiency ensures the system operates optimally, conserving energy and maintaining the desired performance. The graph shown above shows the duct efficiency with respect to Reynolds number. When the Reynolds number increases the duct efficiency will also increases and vice versa. The maximum duct efficiency is 90 at the maximum Reynolds number of 299.

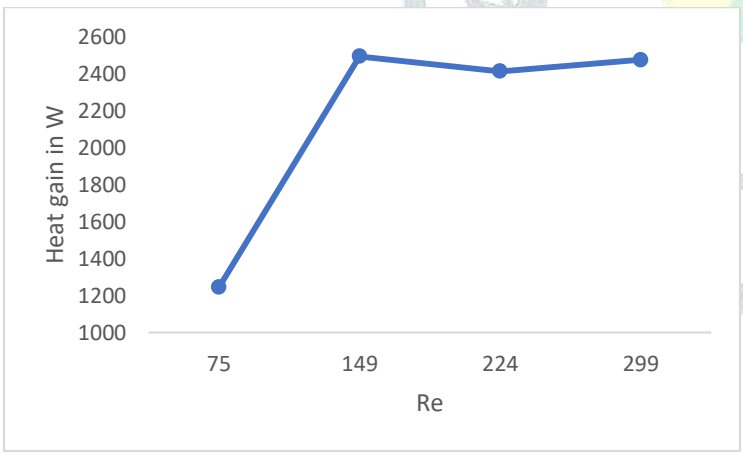

Fig: Heat gain with Re

Heat gain refers to the process of adding heat to a system or an object, causing its temperature to rise. To manage heat gain effectively, it's important to consider factors like insulation, reflective surfaces, ventilation, and heat-absorbing materials, depending on the context in which heat gain is a concern. The graph shown above is the heat gain with respect to Reynolds number. In the graph it is seen that at the beginning the there will be gradual increase in heat gain and at 149 Reynolds numbers there will be constant for increasing Reynolds number.

Conclusion

In this study, a solar air heater utilizing solar energy and a rectangular duct has been devised. The conventional air heating efficiency is enhanced through the incorporation of baffles, including the implementation of perforated baffles. This methodology is executed through both analytical and numerical approaches. On the analytical front, computations are carried out for efficiency, heat gain, friction factor, heat transfer coefficient, and Nusselt number across various mass flow rates. Meanwhile, the numerical aspect employs the ANSYS FLUENT software, specifically conducting laminar flow CFD analysis. This enables the collection of readings for pressure drop and heat transfer coefficient through CFD simulations. Increasing the mass flow rate results in an improvement in the maximum heat transfer coefficient, indicating enhanced performance. Moreover, a correlation is observed between the increase in flow rate and improved overall performance. An augmentation in the friction factor corresponds to a decrease in mass flow rate, contributing to a drop in friction factor. In terms of duct efficiency, higher Reynolds numbers yield improved efficiency, with an approximately 980% efficiency observed at a Reynolds number of 299. However, at a Reynolds number of 75, the duct efficiency stands at 20%. The heat gain is relatively lower at a Reynolds numbers of 75, while a maximum heat gain of 2500 W is observed at a Reynolds number of 299. Notably, there is a strong concurrence between the analytical and numerical findings, exhibiting minimal discrepancies. The design of the solar duct has been manually calculated, and its performance has been verified through CFD simulations. The utilization of baffles and perforated baffles within the solar duct is crucial for enhancing the overall enhancement process.

Reference

[1] Prasad K. and Mullick S. C., 1983, Heat transfer characteristics of a solar air heater used for drying purposes, Applied Energy, 13(2): pp. 83-93.

[2] Prasad B. N. and Saini J. S., 1988, Effect of artificial roughness on heat transfer and friction factor in a solar air heater, Solar Energy, 41(6): pp. 555-560.

[3]. Prasad B. N. and Saini J. S., 1991, Optimal thermo-hydraulic performance of artificially roughened solar air heaters, Solar Energy, 47(2): pp. 91-96.

[4] P.K.Sarma, C.Kedarnath, V.Dharma Rao, P.S.Kishore,T.Subrahmanyam and A.E.Bergles, “Evaluation of Momentum and Thermal Eddy Diffusivities for Turbulent Flow in Tubes”,International Journal of Heat and Mass Transfer, Vol. 53, Issues 5-6, pp.1237-1242, 2010.

[5] P. S. Kishore, “Experimental and theoretical studiesof convective momentum and heat transfer in tubes wth twisted tape inserts, Ph.D thesis, Andhra University visakhapatnam, 2001.

[6] P.K.Sarma, C.Kedarnath, K.V.Sharma, L.Syam Sundar P.S.Kishore and V.Srinivas, “Experimental Study to Predict Momentum and Thermal Diffusivities from Convective Heat Transfer Data of Nano Fluid with Al_2O_3 Dispersion”, International Journal of Heat and Technology, Vol. 28, pp. 123-131, 2010.